Quantum Science and Technology

LETTER • OPEN ACCESS

Synthetic lattices, flat bands and localization in Rydberg quantum simulators

To cite this article: Maike Ostmann *et al* 2019 *Quantum Sci. Technol.* **4** 02LT01

Quantum Science and Technology

LETTER

Synthetic lattices, flat bands and localization in Rydberg quantum simulators

Maike Ostmann[1,2,4], **Matteo Marcuzzi**[1,2], **Jiří Minář**[1,2,3] **and Igor Lesanovsky**[1,2]

[1] School of Physics and Astronomy, University of Nottingham, Nottingham NG7 2RD, United Kingdom
[2] Centre for the Mathematics and Theoretical Physics of Quantum Non-equilibrium Systems, University of Nottingham, Nottingham NG7 2RD, United Kingdom
[3] Department of Physics, Lancaster University, Lancaster LA1 4 YB, United Kingdom
[4] Author to whom any correspondence should be addressed.

E-mail: ppxmo@nottingham.ac.uk

OPEN ACCESS

RECEIVED
3 July 2018

REVISED
11 October 2018

ACCEPTED FOR PUBLICATION
21 November 2018

PUBLISHED
9 January 2019

Keywords: rydberg atoms, localization phenomena, disordered systems, synthetic lattices

Supplementary material for this article is available online

Abstract

The most recent manifestation of cold Rydberg atom quantum simulators that employs tailored optical tweezer arrays enables the study of many-body dynamics under so-called facilitation conditions. We show how the facilitation mechanism yields a Hilbert space structure in which the many-body states organize into synthetic lattices which feature in general one or several flat bands and may support immobile localized states. We focus our discussion on the case of a ladder geometry for which we analyze the influence of disorder generated by the uncertainty of the atomic positions. The localization properties of this system are characterized through two length scales (localization lengths) which are found to display anomalous scaling behavior at certain energies. Moreover, we discuss the experimental preparation of an immobile localized state, and analyze disorder-induced propagation effects.

Introduction

Over the past few decades, advances in the manipulation of cold atomic gases rendered them viable as a versatile quantum simulation platform [1, 2]. Several paradigmatic many-body models have been studied experimentally, including Luttinger liquids [3], Tonks–Girardeau gases [4], Bose–Hubbard [5, 6] and Fermi–Hubbard Hamiltonians [7], permitting to directly observe phenomena such as quantum revivals [8], Lieb–Robinson bounds [9], or topological phase transitions [10].

Among different physical systems apt to act as quantum simulators, ensembles of Rydberg atoms [11–13] stand out for their strong interactions, which give rise to an intricate phenomenology, including devil's staircases [14–16], aggregate formation and melting [17, 18], Rydberg crystals [19], optical bistability [20, 21], phase transitions [22–24] and protected zero modes [25]. These systems are currently employed for a variety of tasks, such as quantum information processing [26–28] and simulation of quantum spin systems [19, 29]. Several among these instances employ the so-called *facilitation* (or *anti-blockade*) mechanism (see e.g. [30–36]), meaning that Rydberg states can only be excited next to an already existing excitation, actuating a form of quantum transport.

In quantum systems, transport can be heavily affected by the presence of quenched disorder via *Anderson localization* [37]. In the presence of randomly-distributed impurities in a metal, for example, different paths taken by an electron can interfere destructively, leading to spatial localization of its wavefunction. In one and two dimensions, this effect is so relevant that for arbitrarily small disorder all energy eigenstates are localized and transport is effectively impossible [38, 39]. These effects have been experimentally observed in a range of systems, spanning electron gases [40], cold atoms [41–43], thin films [44] and periodically-driven nitrogen molecules [45].

Apart from the case of quenched disorder, localized states can also arise in tight-binding models from particular lattice geometries. In these cases, destructive interference comes not from the random nature of the phases acquired along different trajectories, but from a specific careful arrangement of the lattice, and leads to the emergence of flat bands. Models with flat bands typically allow the construction of localized eigenstates, and have been experimentally realized with cold atoms [46], photonic lattices [47], and synthetic solid-state structures [48, 49]. When disorder is introduced in such systems, these pre-existing localized states couple to the dispersive, delocalized ones and start acting like scatterers. The ensuing richer phenomenology includes localization enhancement [50], Anderson transitions in lower-dimensional systems [51], and disorder-induced delocalization [52].

In this paper we demonstrate that Rydberg lattice quantum simulators [19, 29, 53] permit the exploration of these anomalous disorder phenomena. We show that under facilitation conditions the Hilbert space acquires a regular (synthetic) lattice structure supporting flat bands. In this picture, the uncertainty of atomic positions translates into a disordered potential acting on its sites. Similar scenarios were previously theoretically analyzed in [50, 51]. Here we show that they emerge naturally in Rydberg quantum simulators employing optical tweezer arrays [29, 53, 54]. We illustrate our findings for the case of a so-called 'Lieb ladder'. We analyze the scaling of the localization lengths and discuss the spreading dynamics of a local flat-band eigenstate under the action of different disorder strengths.

Facilitation, Hilbert space structure and flat bands

We consider a regular[5] lattice of N optical tweezers, each loaded with a single Rydberg atom, and with nearest-neighbor distance R_0. A laser is shone with a frequency detuned by Δ with respect to an atomic transition between the electronic ground state $|\downarrow\rangle$ and a Rydberg level $|\uparrow\rangle$. We work here in natural units $\hbar = 1$. Atoms in the Rydberg state $|\uparrow\rangle$ interact, at distance d, via an algebraically-decaying potential $V(d) = C_\alpha/d^\alpha$, with $\alpha = 3$ (6) for dipole-dipole (van-der-Waals) interactions (without loss of generality we choose $C_\alpha > 0$). Within the rotating wave approximation the Hamiltonian of this system reads

$$\hat{\mathrm{H}} = \Omega \sum_{k=1}^{N} \hat{\sigma}_x^{(k)} + \Delta \sum_{k=1}^{N} \hat{\mathrm{n}}_k + \frac{1}{2} \sum_{\substack{k=1 \\ m\neq k}}^{N} V(d_{km})\, \hat{\mathrm{n}}_m\, \hat{\mathrm{n}}_k, \tag{1}$$

where Ω is the laser Rabi frequency, k and m are lattice indices, d_{km} denotes the distance between atoms in sites k and m, $\hat{\sigma}_x^{(k)} = |\uparrow_k\rangle\langle\downarrow_k| + |\downarrow_k\rangle\langle\uparrow_k|$ and $\hat{\mathrm{n}}_k = |\uparrow_k\rangle\langle\uparrow_k|$. The facilitation condition is obtained by setting $\Delta = -V(R_0)$, so that an isolated excited atom makes its neighbors' transitions resonant with the laser. In the following, we consider $|\Delta| \gg \Omega$, so that non-facilitated atoms are sufficiently off-resonant to neglect their excitation. Furthermore, we require $V(2R_0) \gg \Omega$ which implies that a pair of neighboring excitations is unable to facilitate any nearby site. Neglecting these strongly suppressed transitions effectively splits the Hilbert space into subspaces separated by energy scales $\gg\Omega$ [55, 56]. Each subspace comprises a set of 'quasi-resonant' states separated by scales $\sim O(\Omega)$ (see [56] for more details). Intuitively, this means that an isolated excitation can at most produce one more in the neighborhood, after which either the former facilitates the de-excitation of the latter, or vice versa:

$$|\ldots\downarrow\uparrow\downarrow\downarrow\ldots\rangle \overset{\hat{\mathrm{H}}}{\longleftrightarrow} |\ldots\downarrow\uparrow\uparrow\downarrow\ldots\rangle \overset{\hat{\mathrm{H}}}{\longleftrightarrow} |\ldots\downarrow\downarrow\uparrow\downarrow\ldots\rangle. \tag{2}$$

Here we work in the simplest non-trivial subspace, which contains all configurations with either a single excitation or a single pair of neighboring ones, whose states can be obtained by repeatedly applying the Hamiltonian to, e.g. a state with a single excitation at one end of the chain via the mechanism highlighted above. In the following, we will be interested in reconstructing the connectivity structure of these states in the Hilbert space; we shall therefore imagine that each classical (i.e. eigenstate of all $\hat{\sigma}_z^{(k)}$ s) spin configuration is represented by a lattice site, while we identify as 'nearest neighbors' those states which are connected by the Hamiltonian (i.e. $\langle A|\hat{\mathrm{H}}|B\rangle \neq 0$). To avoid confusion, we shall refer to this emerging lattice structure as the *synthetic lattice*, calling instead *real lattice* the one formed by the actual traps. The construction of the synthetic lattice is schematically expounded in figure 1 and can be performed pictorially in a few steps: (i) first, we recognize that there is a one-to-one correspondence between states with a single excitation and the position of that excitation in the real lattice; hence, we dispose these state of the synthetic lattice in the same structure adopted by the real lattice (i.e. in a square ordering if the traps form a square lattice); (ii) second, for later convenience we draw links between each pair of neighbors in this partial structure. (iii) Third, we see from (2) that the Hamiltonian does not directly

[5] We use here the term 'regular' in a loose sense to denote lattices in which each site can be virtually connected to any other by a path of links between nearest neighbors at distance R_0. For instance, in a vertically-elongated rectangular lattice only pairs of points on the same row could be connected this way. Physically, this translates in the ability of a single excitation to propagate to any point in the original array.

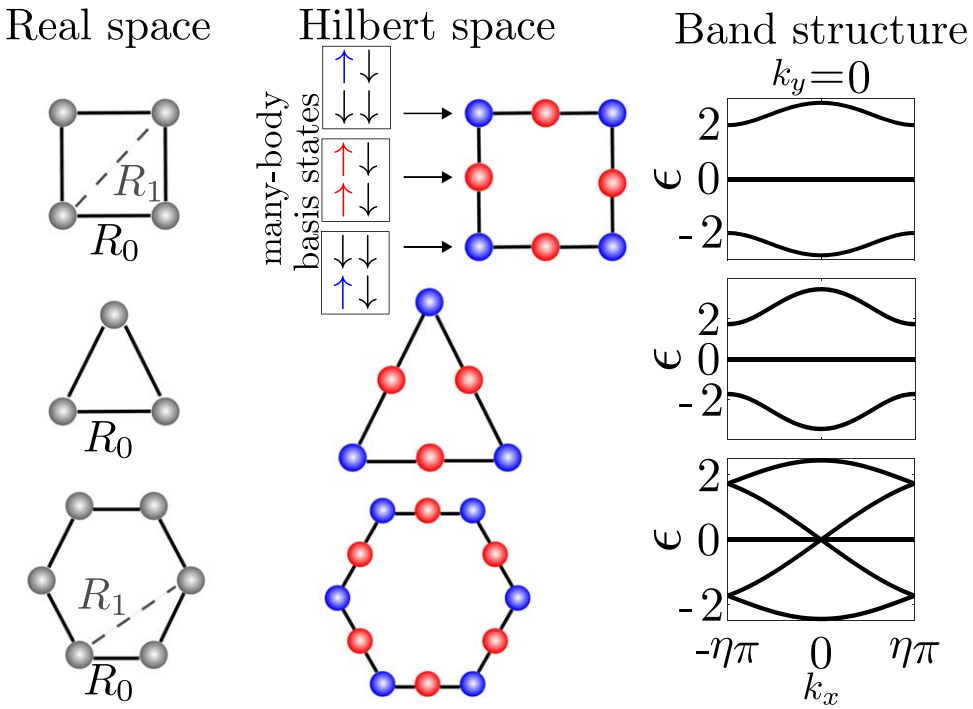

Figure 1. Left column: basic local site configuration within a square, a triangular, and a honeycomb lattices. The gray dots depict the positions of the optical tweezers, while the lines provide a guide to the eye. R_0 and R_1 represent nearest and next-nearest neighbor distances, respectively. Middle column: respective 'synthetic lattices' in the Hilbert space under facilitation conditions. The blue dots represent one-excitation states while the red ones are pair states. Right column: cut through the Brillouin zone for each lattice geometries at $k_y = 0$. Each lattice features (at least) a flat band. The momentum scales for the three lattices (from top to bottom) are $\eta = \left(1, \frac{4}{3}, \frac{4}{3}\right)$.

connect any pair of states with a single excitation, implying that in this partial structure (we are still missing the two-neighboring-excitation, or *pair*, states) no nearest neighbors (according to our definition above) can be found; (iv) from (2) again, we see that single excitation states are indirectly connected by pair states; furthermore, each pair state connects *exclusively* to the two states with a single excitation in either of the positions of the pair. Finally, these two states have excitations in contiguous positions and are therefore, by (ii), connected by one of the links we drew. Hence, we add an extra synthetic lattice site, representing a pair state, on the midpoint of each link, exhausting the states in the subspace and therefore completing the synthetic lattice. For a square lattice, the new structure (see figure 1) is the *Lieb lattice* and is known to feature one flat and two dispersive bands which meet with linear dispersion at the edges of the first Brillouin zone. With an eye to this Dirac-cone-like band structure, this lattice has been theoretically studied before in [57], although in a framework where the Lieb lattice is directly realized by the traps. The construction we summarized above is general and can be extended to any kind of regular lattice (see footnote 5). Most choices will support flat bands as well: it can be shown[6] that, calling n_1 (n_2) the number of one-excitation (pair) states in a unit cell, the number of flat bands $n_{\text{flat}} \geqslant |n_1 - n_2|$. For the square, triangular and honeycomb lattices in figure 1, $(n_1, n_2, n_{\text{flat}}) = (1, 2, 1), (1, 3, 2)$ and $(2, 3, 1)$ respectively. These flat bands constitute extensively-degenerate eigenspaces of the Hamiltonian; as such, it is often possible to recombine the usual (plane-wave-like) Bloch solutions to form a set of localized eigenstates.

Disorder

Disorder enters the picture through the uncertainty in the atomic positions. Even small displacements from the center of the traps can significantly shift the atomic transitions off resonance from the laser frequency, thereby hindering the facilitation mechanism [56]. The interaction potential experienced by an atom at a distance $R = R_0 + \delta R$ from an excitation will be $V(R) = V(R_0 + \delta R) \equiv V(R_0) + \delta V$, with δV representing the random shift. These random variables create an alternating disordered potential landscape over the synthetic lattice which only affects pair (red) sites (see figure 1). The properties of the (correlated) probability distribution are discussed elsewhere (see footnote 6).

To characterize the disorder, we denote by ω the optical tweezer trapping frequency (assumed hereafter to be isotropic in space), by m the atomic mass and by T the temperature. The probability distribution of a trapped

[6] See supplemental material available online at stacks.iop.org/QST/4/02LT01/mmedia.

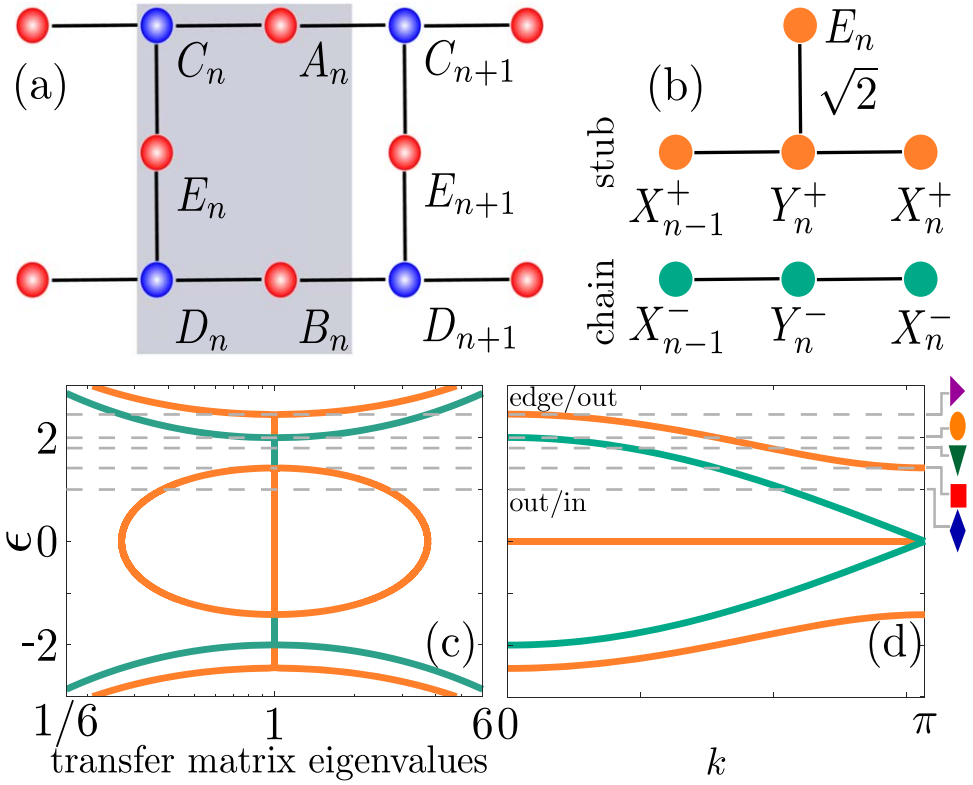

Figure 2. Hilbert space structure and spectrum in the absence of disorder. (a) Lieb ladder; blue (red) dots correspond to one-excitation (pair) states. We denote by A_n, B_n, C_n, D_n, E_n the five sites in the n-th unit cell (shaded in gray). (b) A change of basis—the so-called 'detangling', introducing the new linear combinations $X_n^{\pm} = (A_n \pm B_n)/\sqrt{2}$ and $Y_n^{\pm} = (C_n \pm D_n)/\sqrt{2}$ [50, 58]—maps the Lieb ladder onto two decoupled chains. The $\sqrt{2}$ factor denotes that the hopping amplitude on the vertical link of each unit cell is amplified by that same amount. (c) Eigenvalues of the transfer matrix in log-linear scale. The dotted lines corresponds to the energies $\epsilon = \{1, \sqrt{2}, 1.8, 2, \sqrt{6}\}$ at which the scaling of the localization lengths is investigated in figure 3. (d) Band structure of the Lieb ladder. The bands corresponding to the stub lattice are given in orange and bands of the ordinary 1D chain are shown in green.

atom can then be approximately described as a Gaussian of width σ around the trap center. We require now that (I) $k_B T \gg \hbar\omega$: this implies that one can use the semiclassical estimate $\sigma \approx \sqrt{k_B T/m\omega^2}$ (see footnote 6) and moreover that the thermal de Broglie wavelength of the atom is much smaller than the distribution width. In other words, the atom can be approximately considered localized somewhere within the trap according to a classical probability distribution. (II) $\omega\Delta t \ll 1$, with Δt the duration of an experiment: this ensures that the atoms will not appreciably move from their positions in this time frame and thus the disorder is quenched. (III) $\Omega\Delta t \gtrsim 1$: the internal degrees of freedom are much faster than the kinetic ones, so that within an experimental run the dynamics induced by the disordered Hamiltonian can be probed. One sees, in particular, that (II) and (III) imply that $\Omega/\omega \gg 1$. While challenging, a regime of this kind is in principle reachable. For instance, in [56] this ratio is of order 10 (if one takes, as an upper bound, ω from the short side of the elongated traps). In the supplemental of [56] the role of interatomic repulsion is also discussed and shown to be of the same order of thermal motion, in which case it can be similarly reduced by reducing Δt.

Disordered Lieb ladder

In the remainder of our discussion, we shall focus on a ladder configuration, i.e. a quasi-one-dimensional lattice formed by two parallel linear chains at a distance R_0. For this example, the synthetic lattice (a '1D Lieb lattice') in the Hilbert space is sketched in figure 2(a). The unit cell consists of five sites with $n_1 = 2$ and $n_2 = 3$ and the band structure features one zero-energy flat band and four dispersive ones (figure 2(d)).

This Lieb ladder constitutes one of the simplest examples where flat bands produce a non-trivial interplay with the on-site disorder [50]. In a Rydberg quantum simulator, however, the disorder only appears on pair states, i.e. all the one-excitation (blue in figures 1 and 2) sites of the synthetic lattice are unaffected by it. To investigate the effect of this unusual disorder scenario we study in the following the scaling behavior of the *localization length* ξ for small disorder strengths. This quantity encodes the localization properties of the energy eigenstates, whose amplitude is typically peaked somewhere within the lattice and decays exponentially as $e^{-r/\xi}$ at large distances r.

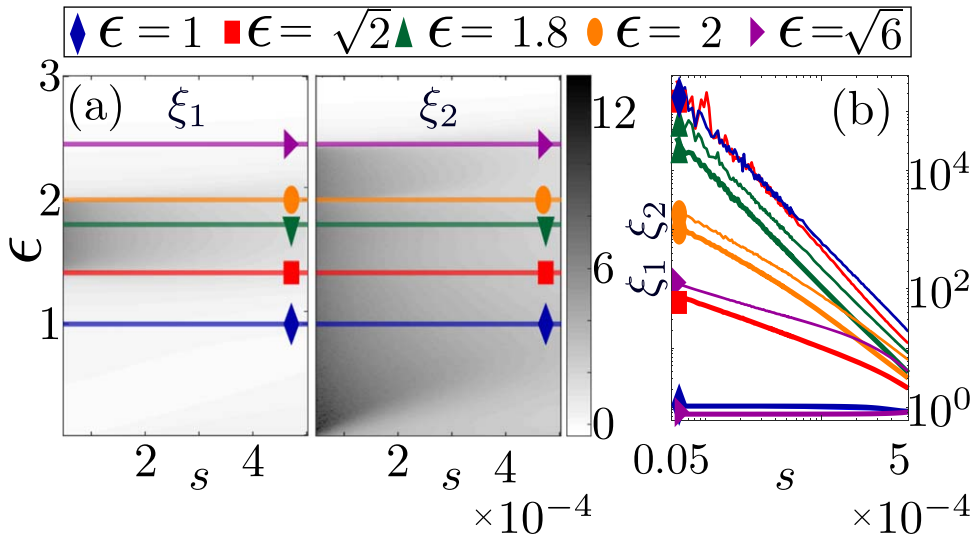

Figure 3. (a) Localization lengths ξ_1, ξ_2 as a function of the energy ϵ and the disorder strength $s = \sigma/R_0$. (b) Localization lengths ξ_1 (thick lines), ξ_2 (thin lines) in log-log scale for five different values of the energy, reported above the panel and highlighted in (a) via horizontal, solid lines. For small disorder all curves are approximately linear, making it possible to assign power law exponents ν characterizing the small disorder behavior $\xi_i \sim s^{\nu}$: grouping them by energy ϵ, they read $\nu(\epsilon = 1) \approx \{0, 2.2\}$, $\nu(\epsilon = \sqrt{2}) \approx \{0.7,\ 2.2\}$, $\nu(\epsilon = 1.8) \approx \{2.0, 1.9\}$, $\nu(\epsilon = 2) \approx \{1.1, 1.1\}$, $\nu(\epsilon = \sqrt{6}) \approx \{0, 0.6\}$. Here we have chosen a dipole-dipole interaction ($\alpha = 3$) with an interaction strength of $V(R_0) = 300\Omega$. It is apparent that the lowermost curves bend down in the rightmost part of panel (b). For the estimation of the slope, we have considered the data between $s = 5 \times 10^{-6}$ and $s = 5 \times 10^{-5}$.

Table 1. Scaling exponents ν for different energies ϵ. Values in the first column are obtained for $\alpha = 3$ and $n = 10^6$, with n being the effective length of the ladder (or, more precisely, the number of random transfer matrices multiplied in sequence, (see footnote 6). Values in the second column have been taken from [50].

	Experimental disorder $s \in [5 \times 10^{-6}, 5 \times 10^{-4}]$	Flat disorder on all sites (A_i, B_i, C_i, D_i, E_i) values from [50]
$\epsilon = 1$	(0, 2.2)	(0,2)
$\epsilon = \sqrt{2}$	(0.7, 2.2)	(2/3, 4/3)
$\epsilon = 1.8$	(2.0, 1.9)	(2,2)
$\epsilon = 2$	(1.1, 1.1)	(2/3, 4/3)
$\epsilon = \sqrt{6}$	(0, 0.6)	(0, 2/3)

For a ladder configuration, two different values of ξ can be extracted at any given energy, which we denote by $\xi_{1/2}$ and order according to $\xi_1 < \xi_2$. To elucidate the reason, one can perform an appropriate change of basis ('detangling transformation' [50, 58]) through which the Lieb ladder is mapped onto two uncoupled one-dimensional lattices (see figure 2(b)), a chain (in green, supporting the two innermost dispersive bands) and a 'stub' lattice (in orange, supporting the flat and two outermost dispersive bands) (see footnote 6). At small disorder, one can thus associate each localization length to either detangled chain.

The localization lengths $\xi_{1/2}$ are found numerically via a transfer matrix formalism (see footnote 6 for details) and are displayed in figure 3(a) as a function of the disorder strength $s \equiv \sigma / R_0$ and the energy ϵ. In figure 3(b) we display log-log plots of $\xi_{1/2}$ at selected energies as functions of s, which illustrate algebraic scaling $\xi_i \sim s^{\nu}$, for sufficiently small s. Where possible, we connect our findings to those presented in [50], where the same geometry is studied with independent disorder on all sites. This is summarized in table 1 (see footnote 6). The usual scaling for Anderson localization corresponds to $\nu = 0$ at energies outside a band ('out'), $\nu = 2/3$ at a band edge ('edge') and $\nu = 2$ inside a band ('in'). The energies selected in figure 2 correspond to $\epsilon = 1$ (out/in), $\sqrt{2}$ (edge/in), 1.8 (in/in), 2 (in/edge) and $\sqrt{6}$ (edge/out). The entries within brackets refer here to the two sets of bands depicted in figures 2(c), (d) (orange/green), again relative to either detangled chain.

In [50] an 'anomalous' scaling $\nu = 4/3$ was found at $\epsilon = \sqrt{2}$ and 2. This was attributed to the fact that disorder, in the detangled picture, is not merely on-site but couples the two chains. This in turn may produce resonances between states in the middle of a band and states at the edge of the other when the latter displays vanishing group velocity. Comparing these values with the ones obtained for our situation, we observe reasonable agreement at $\epsilon = 1$, $\epsilon = 1.8$ and $\epsilon = \sqrt{6}$, plus for the 'edge' scaling at $\epsilon = \sqrt{2}$. The anomalous 'in' scaling at $\epsilon = \sqrt{2}$ seems instead to be 'cured' as we retrieve a result compatible with the usual Anderson one ($\nu \approx 2$). As we argue elsewhere (see footnote 6), this is likely to be due to the alternating structure of the disorder

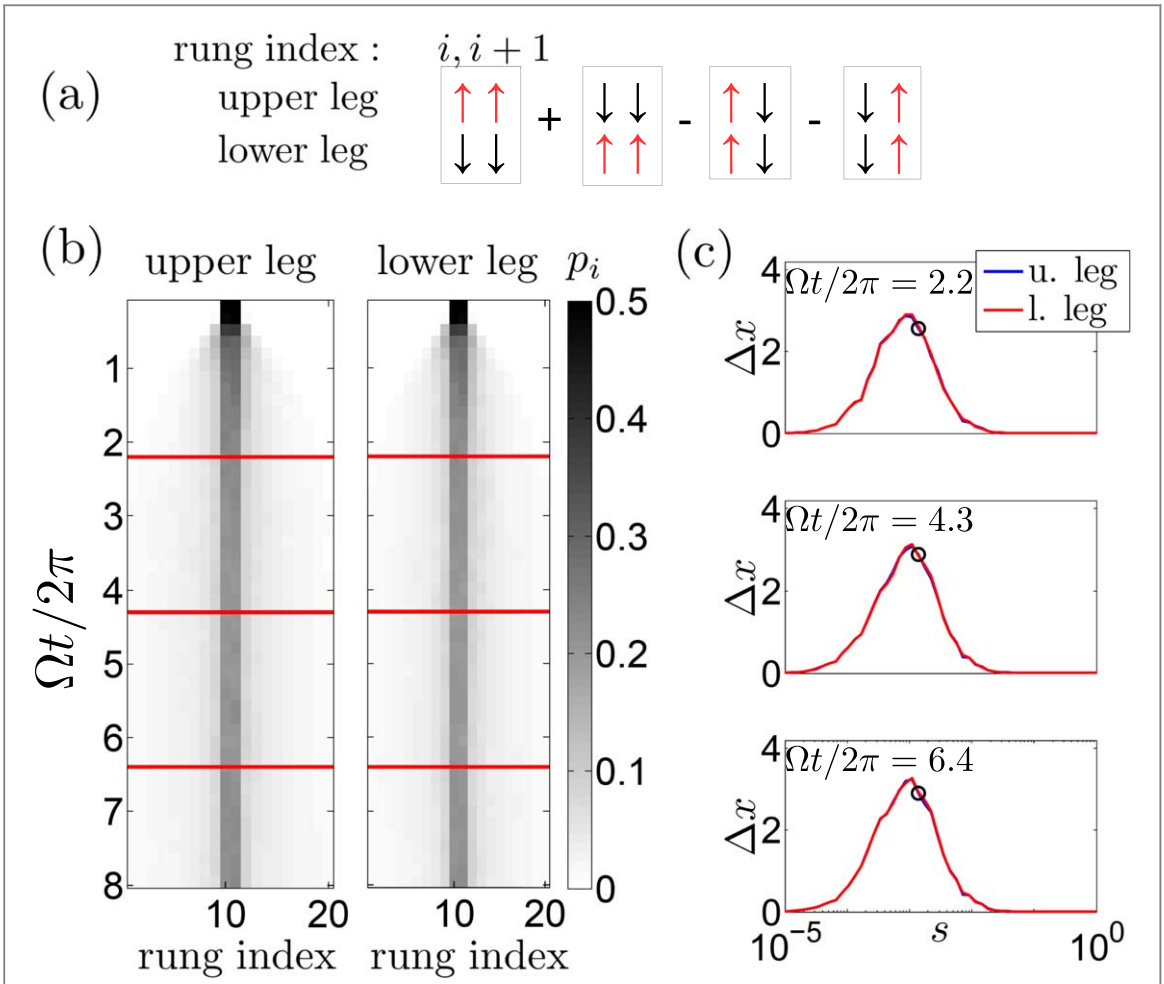

Figure 4. (a) Schematic representation of the spin configuration corresponding to the initial state $|\psi_{\rm loc}\rangle$ localized at rungs $i, i+1$ of the ladder. (b) The averaged probability of excitations p_i given by the time evolution of the localized state with an initial support in the middle (rungs 10 and 11) of the ladder of length 20 for $s = 0.0014$. The left (right) panel shows the time evolution in the upper (lower) leg of the ladder. The horizontal red lines denote three different times for which the respective value of Δx is shown as a black circle in (c). (c) Standard deviation of the excitation positions Δx versus the disorder strength s for three different times. Blue (red) solid lines, which are virtually indistinguishable correspond to upper (lower) leg of the ladder respectively. Results obtained for 100 disorder realizations and $V(R_0) = 200\Omega$.

in the synthetic lattice, which in the detangled picture results in the absence of random couplings between $Y_n^{\pm}$ sites (see figure 2(b)), present instead in [50].

We find however discrepancies at $\epsilon = 2$, where both localization lengths are close to 1.1 and do not seem to match with either of the expected values 2/3 (edge) or 4/3 (in, anomalous). An explanation for this behavior, which does not seem to be related simply to the alternating structure of the disorder (see footnote 6), is currently lacking and requires further investigations.

Localized flat band state dynamics

Experimentally measuring the localization lengths studied above is challenging due to the required large system size and small disorder amplitudes. However, one can probe the influence of disorder by initializing the system in a specific state and tracking the subsequent dynamics by measuring the on-site excitation densities $\langle \hat{n}_i \rangle$ [19, 29, 53]. A particularly interesting choice for an initial state is one of the localized eigenstates of the flat band. Such state is immobile in the absence of disorder. We show elsewhere (see footnote 6) that it takes the form $|\psi_{\rm loc}\rangle = 1/\sqrt{4}\,(|A_i\rangle + |B_i\rangle - |E_i\rangle - |E_{i+1}\rangle)$, being entirely localized between the i-th and $(i+1)$-th rungs of the ladder (see figure 4(a)). States of this form can be prepared experimentally via single site addressing (see footnote 6).

The time evolution of the excitation density is shown in figure 4(b). The effect of the disorder becomes apparent in the width Δx (see footnote 6) of the density packet which quickly reaches a stationary state. It is interesting to observe that, as shown in figure 4(c), the stationary value of Δx displays a non-monotonic behavior as a function of s. This can be understood as follows: at very small (but finite) disorder strength s the

initial state (energy $\epsilon \approx 0$) is almost a flat band eigenstate and it therefore only minimally spreads (see e.g. [52, 59]). As s is increased this state hybridizes with other ones, either neighboring localized states with which it acquires an overlap, or delocalized ones, allowing transport over larger distances to occur. At the same time, however, the localization lengths at $\epsilon \approx 0$ decrease. Since the latter bound the maximal spreading Δx of the state, once the decrease in the localization scale catches up with the increase of Δx, the behavior is dominated by localization and, as expected, Δx decreases with increasing disorder strength.

Conclusions and outlook

We have shown that Rydberg quantum simulators allow to explore localization phenomena in synthetic lattices with flat bands and unconventional types of disorder (correlated, alternating). The current study focuses on the Lieb ladder and on a particular excitation sector. Key features of the phenomenology discussed for this case are however more general and would apply to higher-dimensional lattices as well. In particular, these would give rise to effective synthetic lattices with flat bands and localized eigenstates capable of aiding the localization. In two dimensions, a similar behavior to the one observed in the Lieb ladder is expected to occur, whereas in three, according to the standard properties of Anderson localization, a transition is expected at some disorder strength from a regime that allows transport to a fully-localized one, related to the appearance of mobility edges in the spectrum. These higher-dimensional cases are realizable with current experimental techniques, making it a theoretical challenge to shed light on these more intricate scenarios.

Acknowledgments

The research leading to these results has received funding from the European Research Council under the European Unions Seventh Framework Programme (FP/2007-2013)/[ERC Grant Agreement No. 335266, (ESCQUMA)]; the Engineering and Physical Sciences Research Council [Grant No. EP/M014266/1]; and the H2020 FETPROACT 2014 [Grant No. 640378 (RYSQ)]. IL gratefully acknowledges funding through the Royal Society Wolfson Research Merit Award.

ORCID iDs

Maike Ostmann https://orcid.org/0000-0001-7423-6559
Igor Lesanovsky https://orcid.org/0000-0001-9660-9467

References

[1] Bloch I, Dalibard J and Zwerger W 2008 *Rev. Mod. Phys.* **80** 885
[2] Bloch I, Dalibard J and Nascimbene S 2012 *Nat. Phys.* **8** 267
[3] Hofferberth S, Lesanovsky I, Schumm T, Imambekov A, Gritsev V, Demler E and Schmiedmayer J 2008 *Nat. Phys.* **4** 489
[4] Kinoshita T, Wenger T and Weiss D S 2004 *Science* **305** 1125
[5] Greiner M, Mandel O, Esslinger T, Hänsch T W and Bloch I 2002 *Nature* **415** 39
[6] Greiner M, Mandel O, Rom T, Altmeyer A, Widera A, Hänsch T and Bloch I 2003 *Physica* B **329** 11
[7] Köhl M, Moritz H, Stöferle T, Günter K and Esslinger T 2005 *Phys. Rev. Lett.* **94** 080403
[8] Greiner M, Mandel O, Hänsch T W and Bloch I 2002 *Nature* **419** 51
[9] Cheneau M, Barmettler P, Poletti D, Endres M, Schauß P, Fukuhara T, Gross C, Bloch I, Kollath C and Kuhr S 2012 *Nature* **481** 484
[10] Hadzibabic Z, Krüger P, Cheneau M, Battelier B and Dalibard J 2006 *Nature* **441** 1118
[11] Saffman M, Walker T and Mølmer K 2010 *Rev. Mod. Phys.* **82** 2313
[12] Löw R, Weimer H, Nipper J, Balewski J B, Butscher B, Büchler H P and Pfau T 2012 *J. Phys.* B **45** 113001
[13] Gallagher T F (ed) 1994 *Rydberg Atoms* (Cambridge: Cambridge University Press)
[14] Weimer H and Büchler H P 2010 *Phys. Rev. Lett.* **105** 230403
[15] Levi E, Minář J and Lesanovsky I 2016 *J. Stat. Mech.* 033111
[16] Lan Z, Minář J, Levi E, Li W and Lesanovsky I 2015 *Phys. Rev. Lett.* **115** 203001
[17] Schempp H *et al* 2014 *Phys. Rev. Lett.* **112** 013002
[18] Lan Z, Li W and Lesanovsky I 2016 *Phys. Rev.* A **94** 051603
[19] Schauß P, Zeiher J, Fukuhara T, Hild S, Cheneau M, Macrì T, Pohl T, Bloch I and Groß C 2015 *Science* **347** 1455
[20] Carr C, Ritter R, Wade C G, Adams C S and Weatherill K J 2013 *Phys. Rev. Lett.* **111** 113901
[21] Šibalić N, Wade C G, Adams C S, Weatherill K J and Pohl T 2016 *Phys. Rev.* A **94** 011401
[22] Löw R, Weimer H, Krohn U, Heidemann R, Bendkowsky V, Butscher B, Büchler H P and Pfau T 2009 *Phys. Rev.* A **80** 033422
[23] Marcuzzi M, Levi E, Diehl S, Garrahan J P and Lesanovsky I 2014 *Phys. Rev. Lett.* **113** 210401
[24] Gutiérrez R, Garrahan J P and Lesanovsky I 2015 *Phys. Rev.* E **92** 062144
[25] Schecter M and Iadecola T 2018 *Phys. Rev.* B **98** 035139
[26] Jaksch D, Cirac J I, Zoller P, Rolston S L, Côté R and Lukin M D 2000 *Phys. Rev. Lett.* **85** 2208
[27] Weimer H, Müller M, Lesanovsky I, Zoller P and Büchler H P 2010 *Nat. Phys.* **6** 382
[28] Saffman M 2016 *J. Phys.* B **49** 202001

[29] Labuhn H, Barredo D, Ravets S, de Léséleuc S, Macrì T, Lahaye T and Browaeys A 2016 *Nature* **534** 667
[30] Ates C, Pohl T, Pattard T and Rost J M 2007 *Phys. Rev. Lett.* **98** 023002
[31] Amthor T, Giese C, Hofmann C S and Weidemüller M 2010 *Phys. Rev. Lett.* **104** 013001
[32] Gärttner M, Heeg K P, Gasenzer T and Evers J 2013 *Phys. Rev.* A **88** 043410
[33] Schönleber D W, Gärttner M and Evers J 2014 *Phys. Rev.* A **89** 033421
[34] Lesanovsky I and Garrahan J P 2014 *Phys. Rev.* A **90** 011603
[35] Urvoy A, Ripka F, Lesanovsky I, Booth D, Shaffer J P, Pfau T and Löw R 2015 *Phys. Rev. Lett.* **114** 203002
[36] Valado M M, Simonelli C, Hoogerland M D, Lesanovsky I, Garrahan J P, Arimondo E, Ciampini D and Morsch O 2016 *Phys. Rev.* A **93** 040701
[37] Anderson P W 1958 *Phys. Rev.* **109** 1492
[38] Mott N and Twose W 1961 *Adv. Phys.* **10** 107
[39] Ishii K 1973 *Prog. Theor. Phys. Suppl.* **53** 77
[40] Cutler M and Mott N F 1969 *Phys. Rev.* **181** 1336
[41] Billy J, Josse V, Zuo Z, Bernard A, Hambrecht B, Lugan P, Clément D, Sanchez-Palencia L, Bouyer P and Aspect A 2008 *Nature* **453** 891
[42] Roati G, D'Errico C, Fallani L, Fattori M, Fort C, Zaccanti M, Modugno G, Modugno M and Inguscio M 2008 *Nature* **453** 895
[43] Semeghini G, Landini M, Castilho P, Roy S, Spagnolli G, Trenkwalder A, Fattori M, Inguscio M and Modugno G 2015 *Nat. Phys.* **11** 554
[44] Liao J *et al* 2015 *Phys. Rev. Lett.* **114** 216601
[45] Bitter M and Milner V 2016 *Phys. Rev. Lett.* **117** 144104
[46] Taie S, Ozawa H, Ichinose T, Nishio T, Nakajima S and Takahashi Y 2015 *Sci. Adv.* **1** 1–7, http://advances.sciencemag.org/content/1/10/e1500854.full.pdf
[47] Mukherjee S, Spracklen A, Choudhury D, Goldman N, Öhberg P, Andersson E and Thomson R R 2015 *Phys. Rev. Lett.* **114** 245504
[48] Slot M R, Gardenier T S, Jacobse P H, van Miert G C, Kempkes S N, Zevenhuizen S J, Smith C M, Vanmaekelbergh D and Swart I 2017 *Nat. Phys.* **13** 672
[49] Drost R, Ojanen T, Harju A and Liljeroth P 2017 *Nat. Phys.* **13** 668
[50] Leykam D, Bodyfelt J D, Desyatnikov A S and Flach S 2017 *Eur. Phys. J.* B **90** 1
[51] Bodyfelt J D, Leykam D, Danieli C, Yu X and Flach S 2014 *Phys. Rev. Lett.* **113** 236403
[52] Goda M, Nishino S and Matsuda H 2006 *Phys. Rev. Lett.* **96** 126401
[53] Bernien H *et al* 2017 *Nature* **551** 579
[54] Jau Y-Y, Hankin A, Keating T, Deutsch I and Biedermann G 2016 *Nat. Phys.* **12** 71
[55] Mattioli M, Glätzle A W and Lechner W 2015 *New J. Phys.* **17** 113039
[56] Marcuzzi M, Minář J, Barredo D, de Léséleuc S, Labuhn H, Lahaye T, Browaeys A, Levi E and Lesanovsky I 2017 *Phys. Rev. Lett.* **118** 063606
[57] Shen R, Shao L B, Wang B and Xing D Y 2010 *Phys. Rev.* B **81** 041410
[58] Flach S, Leykam D, Bodyfelt J D, Matthies P and Desyatnikov A S 2014 *EPL* **105** 30001
[59] Vicencio R A, Cantillano C, Morales-Inostroza L, Real B, Mejía-Cortés C, Weimann S, Szameit A and Molina M I 2015 *Phys. Rev. Lett.* **114** 245503